Supplemental Text for:

In the trenches of real-world self-control:

Neural correlates of breaking the link between craving and smoking

Elliot T. Berkman

University of Oregon

Emily B. Falk

University of Michigan

Matthew D. Lieberman

University of California, Los Angeles

Supplementary Methods

fMRI data acquisition and analysis

Participants were situated in the scanner, where foam padding was placed around their heads to reduce motion. Stimuli were presented on LCD goggles, and responses were recorded on a magnet-safe joystick placed in the right hand (Resonance Technology, Northridge, CA, USA). Participants responded to each go trial by pushing or pulling a lever then clicking a button at the top of the lever. Response time was computed as the latency between stimulus onset and the button click, errors were determined according to trial type, and distance and velocity were calculated based on the position of the lever at the time of the button click.

High-resolution structural T2-weighted echo-planar images (spin-echo; TR = 5000 ms; TE = 34 ms; matrix size 128 x 128; 34 sagittal slices; FOV = 192mm; 4 mm thick) were acquired coplanar with the functional scans. Four functional scans lasting 6:30, 5:46, 5:46 and 5:00 were acquired during the task (echo-planar T2*-weighted gradient-echo, TR = 2000 ms, TE = 30 ms, flip angle = 90°, matrix size 64 x 64, 34 axial slices, FOV = 192 mm; 4 mm thick), totaling 692 functional volumes.

The imaging data were analyzed using a combination of FSL tools (FMRIB Software Library; Oxford University, Oxford, UK) and SPM8 (Wellcome Department of Cognitive Neurology, Institute for Neurology, London, UK). The preprocessing stream for the images was as follows. All images were brain-extracted using BET (FSL's Brain Extraction Tool) and realigned within runs using MCFLIRT (FSL's Motion Correction using FMRIB's Linear Image Registration Tool), then checked for residual motion and noise spikes using a custom automated diagnostic tool (thresholded at 2mm motion or 2% global signal change from one image to the next). In SPM8, all functional and anatomical images were reoriented to set the origin to the

anterior commissure and the horizontal (*y*) axis parallel to the AC-PC line. Also in SPM8, functional images were corrected for slice acquisition timing differences within volumes, realigned within and between runs to correct for residual head motion, and coregistered to the matched-bandwidth structural scan using a 6-parameter rigid body transformation. The coregistered structural scan was then normalized into the Montreal Neurological Institute (MNI) standard stereotactic space and the resulting parameters were applied to all functional images. Finally, the normalized functional images were smoothed using an 8 mm full width at half maximum Gaussian kernel.

One run from each of two participants was removed due to motion. Data from three other participants contained motion spikes that were statistically removed using regressors corresponding to the affected scans.

The design was modeled as an event-related within-subjects one-way ANOVA with response inhibition as a factor with two levels: go and no-go. An implicit baseline condition was comprised of the twelve-second fixation periods that followed each block. Each trial was modeled as an event with 1-second duration and convolved with the canonical hemodynamic response. Temporal autocorrelations in the functional data were addressed using a first-order auto-regressive error structure.

We used a Monte Carlo simulation (AlphaSim; distributed as part of the AFNI Software Package, Medical College of Wisconsin, Milwaukee, WI) to determine that the minimum cluster size necessary to maintain a false detection rate of 5% for a whole-brain search of the [no-go > go] contrast was 20 3x3x3mm voxels combined with a voxel-wise threshold of .001. All functional imaging results are reported in MNI coordinates.

Experience sampling

Participants could silence or disable their phones at their discretion. In the event that they were unable to respond to a prompt before the arrival of the subsequent prompt they were instructed to respond only to the most recent prompt. In other words, participants had roughly two hours to respond to each prompt. Participants were sent a reminder text message or received a phone call if their response rate dropped below 50% for a 24-hour period.

The text message prompts were sent and received through an automated web-based service (RedOxygen Pty. Ltd., Brisbane, Queensland, Australia). Records including the timestamp and content of each message that was sent and received were downloaded from the RedOxygen website.

The Freedom From Smoking cessation program was ongoing from two weeks before the quit date until six weeks following the quit date. Thus, all participants were enrolled in the program for the entire duration of the experience sampling phase of the study.

Time-series data often violates the assumption of sphericity among the dependent measures. To test for this, we used the Hierarchical Multivariate Linear Modeling module of HLM6 to run a nested set of models. The most unrestricted model allowed for all separate variances and covariances within the 8x8 within-day variance-covariance matrix, and more restrictive variance structures such as identical variances but unique covariances and first-order auto-regressive were nested within that model. Deviance change tests suggested that sphericity was met within-days. Nonetheless, we used robust estimates of standard errors with the assumption of over-dispersion to conservatively guard against violations of normality and sphericity (Zeger, Liang, & Albert, 1988).

Integration of fMRI and experience sampling data

To assess which inhibition-related neural activations had prospective predictive value of smoking cessation outcomes, we identified voxels that correlated with overall smoking change from baseline to endpoint within a functional ROI based on significant activations in the no-go > go contrast. This is a relatively conservative approach because these voxels will have reduced variance due to their restricted range (Lieberman, Berkman, & Wager, 2009). False detection rate of .05 was achieved on this analysis using a combined voxel-wise threshold of .01 for each of the conjoined analyses together with a cluster-extent threshold of 20 voxels (Kampe, Frith, & Frith, 2003; Ochsner, Hughes, Robertson, Cooper, & Gabrieli, 2009). To further bolster the predictive power by testing their generalizability to new data, results from this analysis were entered into a leave-one-out cross-validation analysis (Falk, Berkman, Mann, Harrison, & Lieberman, 2010; Stone, 1974). This analysis identified regions in which activation during response inhibition at baseline was predictive of subsequent global success at smoking cessation across a four-week period.

Supplementary Results

Smoking change from baseline to endpoint

Within days, there was a positive relationship between craving at one time point and smoking at the next when craving was entered alone into the model (i.e. without neural activations; log-expectation $\gamma = .19$, $SE = .08$, $t(476) = 2.14$, $p < .05$). Individuals in the upper tertile of this everyday craving-smoking relationship (i.e. those with a strong positive relationship) reduced smoking significantly less (M= 8.50 cigarette reduction/day) than those in the lower tertile (i.e. those with a weak or no relationship between craving and smoking; M=18.44 cigarette reduction/day, $t_{24}=2.22$, $p<.05$).

Predicting everyday response inhibition from neuroimaging data

To explore the differential contributions of the caudate and putamen within the basal ganglia, we ran the analysis separately for left and right ROIs of each of those regions based on the AAL toolbox (Tzourio-Mazoyer, et al., 2002). Activation in the left caudate (log-γ = -.20, p<.04) and the left and right putamen (log-γs = -.17, -.21, ps<.05) moderated the link between craving and smoking. The right caudate slope (log-γ = -.16) was not significantly different from the left caudate slope, but did not meet our significance threshold (p<.14). Together, activation in the bilateral basal ganglia during response inhibition significantly moderated the relationship between craving and smoking (see Table 2).

We ran another set of models to test whether the moderation of the craving-smoking link by activation in the ROIs was higher at greater levels of craving compared to lower levels of craving. To do this, we created a variable that coded for whether cravings were high (3 or 4 out of 4) or low (0, 1 or 2 out of 4), then generated the interaction term between mean-centered versions of this variable and the reports of prior craving. Conceptually, the slope between this variable and smoking tests whether high levels of craving were more related to smoking than low levels of craving. We then tested whether this interaction variable was significantly moderated by activation in our ROIs, conceptually testing whether the moderation of the craving-smoking link by brain activation was moderated by whether cravings were high or low. The results of these tests support the notion that the moderation of the craving-smoking link by neural activation was higher at relatively higher levels of craving: the moderation was significantly greater at high levels of craving (compared to low levels) for all six ROIs (all γs > .2, all p<.05).

Predicting global smoking change from neuroimaging data

We used a functional localizer to identify voxels associated with response inhibition (i.e. [no-go > go]), then searched within these for voxels that were also associated with change in

exhaled carbon monoxide. The only regions that survived this analysis were two clusters in the right basal ganglia, one cluster in the fusiform gyrus, and one cluster on the occipital pole (Table S1; Figure S1). A leave-one-out cross-validation procedure was used to extend the generalizability of this result to new samples. In this procedure, each participant's change in CO from baseline to endpoint was predicted from his or her right basal ganglia activation in [no-go > go] based on a linear statistical model from all other participants. Across iterations, there was a significant positive correlation between predicted and actual CO change, suggesting predictive validity in the neuroimaging data (cross-validated $r = .40$, $R^2 = 16\%$, $p < .05$; Figure S2).

Robustness to missing data

It seems possible that smokers attempting to quit might under-report smoking lapses, thus it is important to check that this potential systematic bias in the missing data (i.e missing not-at-random) does not affect the results. To check the robustness of our data, we generated simulated data under varying degrees of the assumption that participants systematically smoked more when they missed a smoking report. We simulated the data by computing the mean and standard deviation of daily smoking per participant and replaced instances of missing data with these imputed data. We note that this is a highly conservative test of the possibility of under-reporting of smoking because it assumes that each instance of missing data was counted as a lapse. Even if attempting quitters tended to under-report lapses, it still is unlikely that every missed report corresponded to a lapse.

We re-computed the parameter estimates for each of the key ROIs (IFG, preSMA, and basal ganglia) assuming that participants did not smoke more during missed responses compared to completed responses (mean), participants smoked slightly more during missed responses compared to completed responses (+1 SD), and participants smoked significantly more during

missed responses (+2 SD). In every case, the parameter estimates are slightly attenuated though still significant when missing data are imputed with mean, moderate, and high smoking. None of the parameter estimates fall below our significance threshold of $p<.05$, and none change significantly from the value reported in Table 2.

Also, the hypothesis that the parameter estimates are robust to this violation is further supported by the fact that the mean craving at time points immediately prior to completed responses (M=1.73) is not significantly different from the mean craving at time points immediately prior to missed responses (M=1.72, $p>.7$). Both of these analyses demonstrate that missing data did not impact the slope between craving and subsequent smoking.

Supplementary Discussion

Of our three ROIs commonly involved in response inhibition, only basal ganglia activation predicted long-term success in smoking cessation, but all three predicted successful outcomes of the smaller everyday battles between craving and self-control. And the outcomes of these battles—the battles to prevent craving becoming smoking—in turn related to the outcome of the war in terms of overall daily cigarette reduction. The role of rIFG and SMA in these struggles would have been lost if we had only examined the link between neural activation and overall success.

References

Falk, E. B., Berkman, E. T., Mann, T., Harrison, B., & Lieberman, M. D. (2010). Predicting persuasion-induced behavior change from the brain. *Journal of Neuroscience*, 1-21.

Kampe, K. K. W., Frith, C. D., & Frith, U. (2003). "Hey John": signals conveying communicative intention toward the self activate brain regions associated with "mentalizing," regardless of modality. *Journal of Neuroscience, 23*(12), 5258-5263.

Lieberman, M., Berkman, E. T., & Wager, T. (2009). Correlations in Social Neuroscience Aren't Voodoo: Commentary on Vul et al.(2009). *Perspectives on Psychological Science, 4*(3), 299-307.

Ochsner, K. N., Hughes, B., Robertson, E. R., Cooper, J. C., & Gabrieli, J. D. E. (2009). Neural Systems Supporting the Control of Affective and Cognitive Conflicts. *Journal of cognitive neuroscience, 21*(9), 1841-1854.

Stone, M. (1974). Cross-validation choice and assessment of statistical predictions. *Journal of the Royal Statistical Society B, 36*(2), 111-147.

Tzourio-Mazoyer, N., Landeau, B., Papathanassiou, D., Crivello, F., Etard, O., Delcroix, N., et al. (2002). Automated anatomical labeling of activations in SPM using a macroscopic anatomical parcellation of the MNI MRI single-subject brain. *Neuroimage, 15*(1), 273-289.

Zeger, S. L., Liang, K.-Y., & Albert, P. S. (1988). Models for longitudinal data: A generalized estimating equation approach. *Biometrics, 44*(4), 1049-1060.

Supplemental Figure 1 for:

In the trenches of real-world self-control:

Neural correlates of breaking the link between craving and smoking

Elliot T. Berkman

University of Oregon

Emily B. Falk

University of Michigan

Matthew D. Lieberman

University of California, Los Angeles

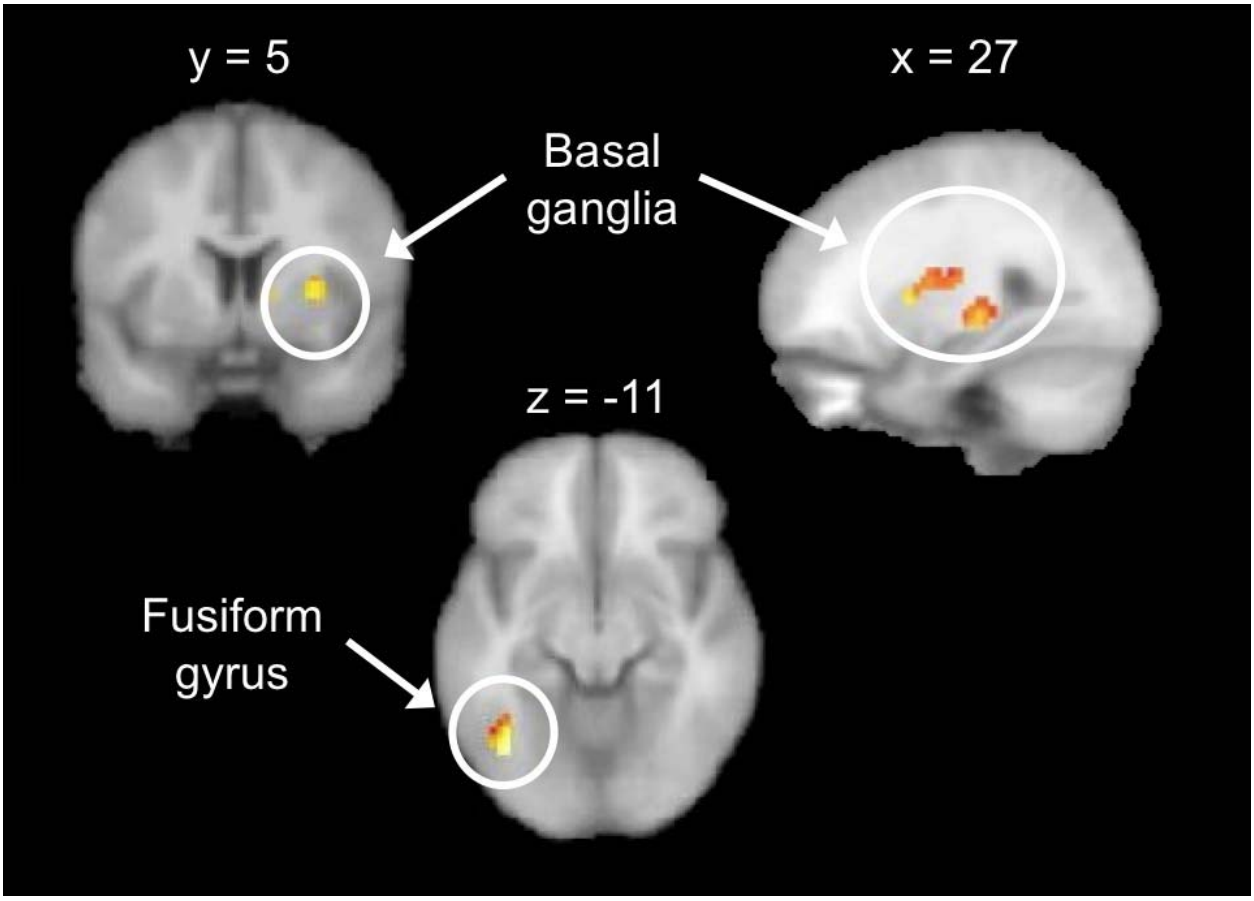

Figure S1. Regions active during the contrast of no-go > go that also correlated with global smoking change (CO from baseline to endpoint). These included the basal ganglia (top; peak MNI: 30 5 4), fusiform gyrus (bottom; -39 -64 -11), and occipital pole (not shown). All activations are FDR corrected at .05.

Supplemental Figure 2 for:

In the trenches of real-world self-control:

Neural correlates of breaking the link between craving and smoking

Elliot T. Berkman

University of Oregon

Emily B. Falk

University of Michigan

Matthew D. Lieberman

University of California, Los Angeles

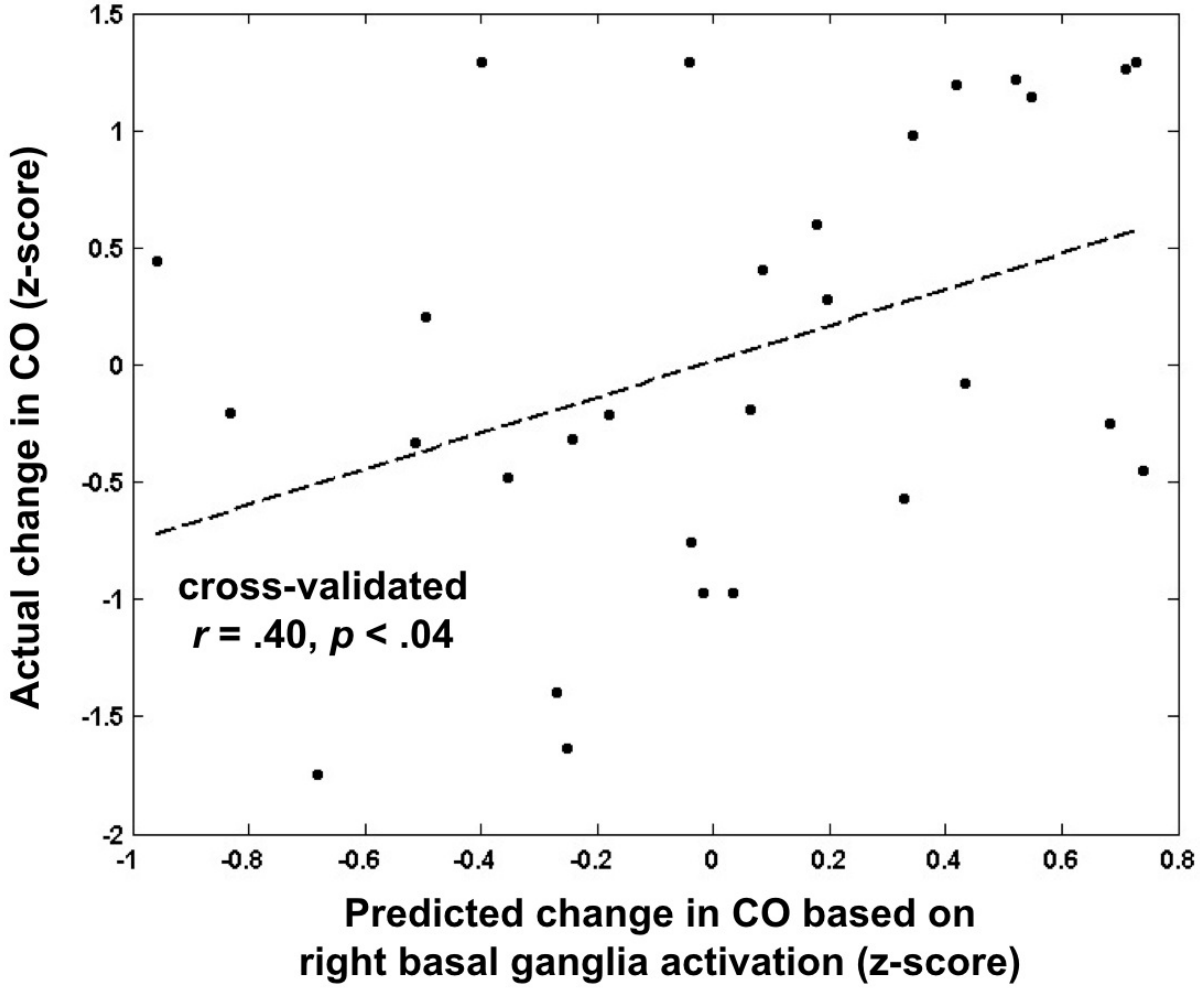

Figure S2. Correlation between actual exhaled carbon monoxide change (from baseline to endpoint) and predictions of change based on neural activation. Iterative leave-one-out cross-validated $r = .40$, $p < .04$.

Table S1

Regions active during [no-go > go] that correlated with change in exhaled CO

Effect	Region	x	y	z	Cluster size	t-val
No-go > go &	Basal ganglia	30	5	4	86	5.02
Positive correlation		30	-16	-2	53	5.78
	Fusiform gyrus	-39	-64	-11	20	6.64
	Occipital pole	-24	-94	10	20	7.57
No-go > go &	*None*					
Negative correlation						

Note. *N*=27. All regions FDR corrected at .05.